AIAA 91-1677
Comparisons of Numerical and Exact Solutions for Oblique Detonations with Structure

J. M. Powers and M. J. Grismer
Department of Aerospace and Mechanical Engineering
University of Notre Dame
Notre Dame, IN

AIAA 22nd Fluid Dynamics, Plasma Dynamics & Lasers Conference
June 24-26, 1991 / Honolulu, Hawaii

COMPARISONS OF NUMERICAL AND EXACT SOLUTIONS FOR OBLIQUE DETONATIONS WITH STRUCTURE

Joseph M. Powers*
Matthew J. Grismer†
University of Notre Dame
Notre Dame, Indiana 46556

Abstract

Numerical predictions of the two-dimensional, inviscid, supersonic, reactive flow of a calorically perfect ideal gas over a straight wedge are compared with the predictions of a linear asymptotic model valid in the hypersonic limit. Solution features predicted by the asymptotic model include a curved shock attached to the wedge tip, a reaction layer parallel to the shock, and a vorticity layer parallel to the wedge surface. For sufficiently high Mach number and heat release, the numerical model predicts similar behavior, and the differences in the predictions of the two methods are of the same order of magnitude as the inherent error of the asymptotic method. As heat release is lowered and Mach number held constant, apparent numerical artifacts obscure features predicted by the asymptotic method. The results suggest that the asymptotic solution has utility as a benchmark to verify the predictions of many high-speed, multi-dimensional, reacting flow codes.

Introduction

Prediction of the the high-speed non-equilibrium flow of a gas over a sharp-edged wedge has been the subject of numerous studies over the past decades. It has become apparent that for the special case of these flows which can be modelled as two-dimensional and inviscid, the basic flow features, as sketched in Fig. 1, can be described as follows. An incoming supersonic equilibrium flow, with a sufficiently high Mach number to prevent shock detachment, encounters a straight wedge inclined at an angle θ. The flow passes through a curved, attached shock. The shock compression initiates non-equilibrium processes which relax to equilibrium in a finite length zone roughly parallel to the lead shock. Near the wedge tip the shock displacement is nearly that of an inert shock; far from the wedge tip the reaction process displaces the shock from its inert position. This variation in shock displacement angle with distance from the wedge tip provides for shock curvature. Consequently, vorticity, proportional to the magnitude of the curvature, is generated at the shock front and is convected in a layer near the wedge surface. The non-equilibrium and vorticity layers both relax to an equilibrium, irrotational uniform state far from the shock and wedge surface. For processes which can be thought of as endothermic, such as vibrational relaxation, the shock is displaced towards the wedge; for exothermic processes such as combustion, the shock is pushed away from the wedge.

The studies of Vincenti[1], which presents closed-form solutions to linearized equations for non-equilibrium flow over a thin wedge, Capiaux and Washington[2], which gives a numerical solution based on the method of characteristics for non-equilibrium flow over a thick wedge, and Lee[3], which presents a closed-form solution for non-equilibrium flow over a thick wedge, are representative of many early studies. With the renewed interest in several hypervelocity devices such as the oblique detonation wave engine[4] (ODWE), the ram accelerator[5], and the advanced hypervelocity aerophysics facility[6] (AHAF), many recent studies have appeared. Among these are those of Bogdanoff and Brackett[7], Fujiwara, et al.[8], Wang, et al.[9], Cambier, et al.[10,11], Yungster[12,13], and Pandolfi, et al.[14] With the exception of the work of Pandolfi, et al., which utilizes the method of characteristics, these studies employ numerical techniques to directly solve the governing partial differential equations. In addition a number of related fundamental and applied studies are cited in the recent book by Anderson[15], which also gives a relevant general discussion.

The topic of this paper is a particular case of non-equilibrium wedge flow known as an oblique detonation with structure. Here an oblique detonation is defined as the flowfield which results when an oblique shock wave induces an exothermic chemical reaction. The term "structure" is used to indicate the flowfield contains spatially thick reaction and vorticity

*Assistant Professor, Department of Aerospace and Mechanical Engineering, Member AIAA.
†Graduate Assistant, Department of Aerospace and Mechanical Engineering, Member AIAA.

layers. Prediction of the variation of physical quantities within the layers requires the solution of differential equations. As such, results from a structure analysis are more rigorous than those obtained by an algebraic Rankine-Hugoniot jump analysis, which assumes heat release occurs in an infinitely thin layer. In particular, solution of the differential equations demonstrates there is a path in phase space to the equilibrium condition, which is presupposed in the Rankine-Hugoniot analysis.

The recent paper of Powers and Stewart[16] gives new closed form oblique detonation solutions. The governing equations employed were the two-dimensional, reactive, Euler equations. The reaction was assumed to be one-step and irreversible with Arrhenius kinetics. Both reactants and products were modelled as calorically perfect ideal gases with identical material properties. This model was studied in the hypersonic limit, linearized about the inert oblique shocked state. In this limit the kinetic energy of the flow is much greater than the heat release from chemical reaction. The leading order solution is the inert shock, and the linear asymptotic theory corrects for the effects of small heat release. Also in this limit the induction zone length is effectively zero; the assumption of large activation energy, which gives rise to a thick induction zone and thin reaction zone, is not made here. Consequently, a simple leading order solution of the kinetic rate law is available. At the following order, acoustic equations with chemical reaction forcing terms generated at leading order are solved to determine the pressure and velocity fields. Two classes of solutions are obtained. The first is irrotational and characterized by a straight shock attached to a curved wedge. The second is rotational and characterized by a curved shock attached to a straight wedge. For the irrotational solutions, it was demonstrated that the differential equations predicted a path to the equilibrium point which was previously identified by a Rankine-Hugoniot analysis.

The solution procedure of Ref. 16 is as follows. To simplify application of the boundary conditions, the Euler equations were first transformed to a non-orthogonal coordinate system fixed to the inert shock and wedge. The equations and shock conditions were then written as linear equations in the hypersonic limit. Assuming the oblique shock was weak and the trailing flow was supersonic allowed the equations to be written in characteristic form. These equations were then solved with the shock position function as a parameter. The shock position function was then specified such that a downstream boundary condition on the wedge surface was met.

In this paper we compare rotational solutions of the linear equations of Ref. 16 to original numerical solutions of their non-linear counterparts. New calculations were necessary as the published oblique detonation solutions (Refs. 7–14) variously employ models of more complex mechanisms such as multistep reactions, non-ideal gases, and viscous transport, or use blunt-nosed wedge geometry. The numerical algorithm is found in the code RPLUS[17,18,19], a general purpose reactive flow code developed at the NASA Lewis Research Center. To our knowledge, these calculations represent the first direct comparisons of the predictions of a linear asymptotic model and a numerical model of the non-linear partial differential equations for an oblique detonation with structure over a straight wedge.

Model Equations

The model equations are taken to be those of Ref. 16. Further justification for the assumptions of this model are given by Fickett and Davis.[20] In dimensionless form the equations are as follows:

$$\frac{\partial}{\partial x}(\rho u) + \frac{\partial}{\partial y}(\rho v) = 0, \tag{1}$$

$$u\frac{\partial u}{\partial x} + v\frac{\partial u}{\partial y} = -\frac{1}{\rho}\frac{\partial P}{\partial x}, \tag{2}$$

$$u\frac{\partial v}{\partial x} + v\frac{\partial v}{\partial y} = -\frac{1}{\rho}\frac{\partial P}{\partial y}, \tag{3}$$

$$u\frac{\partial P}{\partial x} + v\frac{\partial P}{\partial y} - \gamma\frac{P}{\rho}\left(u\frac{\partial \rho}{\partial x} + v\frac{\partial \rho}{\partial y}\right) = \epsilon(\gamma-1)q\rho(1-\lambda)e^{-\epsilon\Theta\rho/P}, \tag{4}$$

$$u\frac{\partial \lambda}{\partial x} + v\frac{\partial \lambda}{\partial y} = (1-\lambda)e^{-\epsilon\Theta\rho/P}, \tag{5}$$

Variables in these equations are the density ρ, Cartesian velocities u and v, pressure P, product mass fraction λ, and Cartesian position coordinates x and y. The parameter ϵ is defined as the reciprocal of the square of the incoming Mach number M_0 ($\epsilon = 1/M_0^2$). In Ref. 16, ϵ is used as a perturbation parameter, while the numerical solutions of this paper make no requirements on the magnitude of ϵ. Other dimensionless parameters are the ratio of specific heats γ, the heat release q, and the activation energy Θ. Equations (1–4) represent conservation of mass, momenta, and energy, respectively. The energy equation (4) incorporates the assumption of a calorically perfect ideal gas. Equation (5) models Arrhenius kinetics and represents a rate law for the product mass fraction. Supplemental but useful equations define the internal energy e, the temperature T, the

sound speed c, and the z component of the vorticity vector ω_z:

$$e = \frac{1}{\gamma - 1}\frac{P}{\rho} - \epsilon\lambda q, \tag{6}$$

$$P = \rho T, \tag{7}$$

$$c = \sqrt{\gamma\frac{P}{\rho}}, \tag{8}$$

$$\omega_z = \frac{\partial v}{\partial x} - \frac{\partial u}{\partial y}. \tag{9}$$

Initial preshock conditions are specified as $\rho = 1$, $u = \sqrt{\gamma}$, $v = 0$, $P = \epsilon$, and $\lambda = 0$.

Solution of the asymptotic model requires the usual Rankine-Hugoniot relations for changes across the inert oblique shock discontinuity. Details are found in Ref. 16. These relations specify discontinuous jumps of pressure, density, and velocity across an oblique shock of specified angle. There is no chemical reaction in this infinitely thin zone; consequently, the product mass fraction remains constant across the shock. For the numerical solution, specification of jump conditions is not required as an appropriate shock capturing scheme is used to spread the discontinuity over a number of cells. To accurately reproduce the asymptotic results, it is important to have sufficient resolution to distinguish a smeared shock and a reaction zone.

The inviscid solution must satisfy the downstream boundary condition of a zero velocity component normal to the wedge surface. In the asymptotic solution of Eqs. (1–9), this is achieved by requiring that the streamline originating at the wedge tip be coincident with the wedge surface. In a somewhat cumbersome process, the shock position function can be chosen such that Eqs. (1–9), along with the initial and shock conditions, describe the flow over a wedge with a specified shape. The numerical method allows for a more straightforward solution. Here, the wedge geometry is directly specified, and the algorithm automatically calculates a compatible shock position and flow field.

Equations (1–9) have been scaled such that in the f ($\epsilon \to 0$) the postshock pressure, density, and velocities are all $O(1)$ quantities. The lengths have been scaled by the reaction zone length. Consequently, both reaction and vorticity layers have $O(1)$ thickness. In terms of dimensional variables (indicated by the notation "~") and dimensional preshock ambient conditions (indicated by the subscript "0"), the dimensionless variables are defined by

$$\rho = \frac{\tilde{\rho}}{\rho_0}, \qquad u = \frac{\tilde{u}}{M_0\sqrt{P_0/\rho_0}},$$

$$v = \frac{\tilde{v}}{M_0\sqrt{P_0/\rho_0}}, \qquad P = \frac{\tilde{P}}{M_0^2 P_0},$$

$$x = \frac{r_0\tilde{x}}{M_0\sqrt{P_0/\rho_0}}, \qquad y = \frac{r_0\tilde{y}}{M_0\sqrt{P_0/\rho_0}}. \tag{10}$$

Remaining dimensionless parameters are defined by the following relations:

$$q = \frac{\rho_0 q_0}{P_0}, \qquad \Theta = \frac{\rho_0 E_0}{P_0}. \tag{11}$$

Here, q_0 is the dimensional heat release, E_0 is the dimensional activation energy, and r_0 is the kinetic rate constant.

Numerical Solution

Numerical solutions for Eqs. (1–9) were obtained with a slightly modified version of the RPLUS reactive flow code. The RPLUS code has the capability to solve the three-dimensional, Reynolds-averaged Navier-Stokes equations and species continuity equations. The code employs the unsteady form of the equations and uses artificially large time steps for accelerated relaxation to a steady-state solution. The code utilizes a finite volume method that is based on the lower-upper symmetric successive overrelaxation (LU-SSOR) implicit factorization scheme. In the RPLUS version used for the present study, the spatial discretization is achieved with central differencing. To avoid oscillations near the shock waves, a combined second-order and fourth-order artificial dissipation term is added. Additional details are given in Ref. 19.

In order to model Eqs. (1–9), the RPLUS code was specified to model inviscid fluid motion with one irreversible reaction. No turbulence modeling was employed. An additional minor modification of the kinetic scheme of RPLUS allowed for a more meaningful comparison. In the hypersonic limit, the exponential factor in the Arrhenius kinetics is unity at leading order. Consequently, the reaction rate is strictly proportional to the mass fraction of reactants. In the asymptotic model of Ref. 16, reaction is allowed only after the material has been shocked. In order to model these kinetics in the numerical solution, the activation energy was arbitrarily set to zero, and an ignition temperature was introduced. The ignition temperature T_{ig}, was defined such that for $T < T_{ig}$, the reaction rate was zero, and for $T > T_{ig}$, the reaction proceeded as dictated by Eq. (5). The ignition temperature was set to a value slightly less than the postshock temperature resulting from an inert oblique shock with the same ambient conditions and wedge geometry. Thus the ignition temperature

serves only as a switch for chemical reaction, and its precise value is not critical.

In addition to the boundary conditions described in the previous section, an additional boundary condition is necessary for the numerical solution at the outflow boundary. This is necessary because of the finite size of the computational domain. For this simulation, the gradient of all flow variables was specified to be zero at the outflow boundary.

All computations were done on an IBM RS/6000 Model 530 with 48 Mbytes of RAM at the University of Notre Dame. A typical computation required approximately 12 hours of CPU time to converge using the grid of 19701 (199 by 99) cell centers depicted in Fig. 2. This was the maximum number of cells that could be used when running the code on the RS/6000. Convergence was achieved in about 2000 pseudo-time steps.

Results and Discussion

The results of two cases are presented here. They are case 1, for which the heat release $q = 10$, and case 2, for which the heat release $q = 1$. For both cases, $\gamma = 1.4$, $M_0 = 20$, and the wedge angle $\theta = 20°$. The RPLUS code requires dimensional input conditions, which were taken to be $P_0 = 101325\ Pa$ and $\rho_0 = 1.1768\ kg/m^3$. The gas was assumed to have the molecular weight of air; consequently, the gas constant was taken to be $R = 287\ J/kg\ K$. For such a high Mach number, many of the assumptions of this model are not valid for common gases found in fuel-air mixtures. Among other things, vibrational relaxation and dissociation become important mechanisms under these conditions. However, as the main purpose of this paper is the verification of a numerical algorithm, these parameters were chosen more for convenience of comparison of results than for reflection of real material behavior.

Contours of mass fraction of product (λ), vorticity (ω_z), and pressure (P) predicted by the asymptotic method are shown in Figs. 3a, 4a, and 5a, respectively. The mass fraction varies monotonically from zero at the shock to near one at an $O(1)$ distance downstream. The shock has a maximum curvature at the wedge tip; it eventually becomes straight and achieves a maximum angle (measured relative to the x-axis) at some $O(1)$ distance above the wedge. Due to this variation in shock curvature, the vorticity is a maximum at the wedge surface, and relaxes monotonically to near zero at some $O(1)$ distance above the wedge. The pressure field is slightly more complicated. Behind the low angle, curved portion of the shock near the wedge tip is a region of low pressure, which increases monotonically along the shock to a high pressure region immediately behind the high angle, straight portion of the the shock. Along the wedge surface, the pressure increases from the low pressure region near the wedge tip to a local maximum pressure, and then slowly decreases in magnitude. This local maximum pressure is less than the pressure immediately following the high angle portion of the shock.

Figures 3b, 4b, and 5b show the numerical results for case 1. In terms of general trends, the results show good agreement. There are minor qualitative differences. First, the numerically predicted shock position is rotated closer to the wedge relative to the asymptotically predicted position. Close examination reveals that the numerical method predicts maximum curvature slightly above the wedge tip, while the asymptotic solution predicts maximum curvature precisely at the wedge tip. Reaction rate contours are qualitatively similar. However, if Fig. 3a is overlayed on Fig. 3b such that the numerical shock position coincides with the asymptotic shock position, it can be seen that the asymptotic solution initially predicts a faster reaction rate than the numerical solution, and then farther downstream predicts a slower rate.

The vorticity contours differ dramatically near the shock and differ slightly downstream of the shock. For the numerical solution, Fig. 4b shows a zone of apparent numerical artifacts around the shock. This is likely attributable to the artificial viscosity spreading the shock over many computational cells. The numerical solution indicates near zero vorticity at the wall which increases rapidly with distance from the wedge to a maximum vorticity region near the wedge surface, and then decreases slowly with distance from the wedge surface to near zero. The maximum vorticity for the numerical case is about half the maximum predicted by the asymptotic solution. At the wedge tip and far above it, the numerical shock is straight, which gives rise to the near zero vorticity at the wall and far above the wedge. It is hypothesized that these differences may be largely due to the effects of artificial viscosity. Near the wedge tip, the distance between the shock and the wedge is of the same order of magnitude as the artificially generated shock width. Consequently, it is unlikely that accurate results are predicted in this region.

Finally, comparing the pressure fields shows that the numerical solution differs from the asymptotic solution by initially predicting a steeper pressure gradient behind the straight portion of the shock. As a result contour levels of the same magnitude are in noticeably different positions. The numerical solution also predicts small closed contours of pressure near the wedge which have no analog in the asymptotic

solution and are apparently numerical artifacts.

Figure 6a,b,c provide a more detailed quantitative comparison between the asymptotic and numerical pressure solutions. In Fig. 6a predictions of pressure on the wedge surface are given for both methods. It is seen that after the numerical method adjusts for the shock over a finite length zone, it tracks the asymptotic solution very accurately. Minor differences apparent in this plot are magnified in Fig. 6b. Here it is seen that the pressure predicted by the numerical method is slightly greater than that predicted by the asymptotic method in the vicinity of the shock. Away from the shock the numerical method consistently predicts slightly lower pressures than the asymptotic method. It is seen that the local, downstream pressure maximum is predicted about 3.5 distance units from the wedge tip by the asymptotic method. This pressure maximum is not predicted by the numerical method. Near the outflow boundary the numerical method predicts small amplitude pressure oscillations on the wedge surface which decrease in magnitude with increasing distance towards the wedge tip. The origin of these disturbances is unclear, though it may involve the behavior of the artificial viscosity model near the wedge surface or the modelling of the outflow boundary condition as a zero-gradient boundary. It is possible that these pressure oscillations have masked the local pressure maximum.

Figure 6c is a semi-log plot of the absolute difference between the asymptotic and numerical pressure predictions along the wedge surface and two other streamwise grid lines of the computational mesh. Their approximate location is indicated in the inset diagram on Fig. 6c. Preceding the shock are the constant ambient conditions, which appear in this figure as the initial regions of very small absolute difference preceding the maximum difference locations. The small differences in this region are due to numerical roundoff and the finite size of the computational cells in the numerical solution. For a given streamwise grid line, the largest maximum differences occur at the shock. There are two likely reasons for this: 1) there is an inherent $O(\epsilon^2)$ error in the shock position predicted by the asymptotic method, and 2) the numerical solution spreads the shock over multiple cells. Following the shock zone is a region of relatively constant difference for all three curves, which has a magnitude of approximately 0.0008. As the error in the asymptotic solution for this case is $O(\epsilon^2) \sim O(0.0025)$, a difference of this magnitude is tolerated. For a rough comparison of the order of magnitude error predicted by the asymptotic method to the actual error, a line of $\epsilon^2 = 0.0025$ is also plotted in Fig. 6c.

For the lower heat release of case 2, the numerical predictions do not agree well with the asymptotic predictions. For this case, the asymptotic method predicts smoothly varying pressure contours as shown in Fig. 8a. These do not match well with the more erratic contours of Fig. 8b, which are predicted by the numerical method. Close examination of continuously shaded color plots of the data reported in Fig. 8b suggests that acoustic waves are propagating within this domain. These apparent numerical artifacts are of the same order of magnitude as the changes in pressure due to the heat release, and thus distort the expected solution. It is likely that these waves originate at the shock or outflow boundary.

Final Remarks

The results of this paper give several insights into the behavior of oblique detonations. First, the numerical calculations suggest, but do not prove, that for the particular cases studied, oblique detonations may be hydrodynamically stable, as the solution relaxes in time to an apparently steady state. The use of artificially large time steps and the use of artificial viscosity, which in addition to dampening numerical instabilities, could potentially dampen physical instabilities, prevents a stronger conclusion. In addition, the effects of finite activation energy, an important ingredient in the well-known detonation instability mechanism[20], are negligible in the hypersonic limit. It is suggested that this contributes to the apparent stability of our results. A more rigorous determination of oblique detonation stability would consider the growth and decay rates of small amplitude disturbances to the steady field. Studies of this type have recently been reported by Jackson, et al.[21] and Lasseigne, et al.[22] for the case of large activation energy. Steady oblique detonations characterized by a straight shock followed by an irrotational flow field containing a thick induction zone and thin chemical reaction zone are considered. They report that a weak upstream vorticity disturbance generates two classes of disturbances: a post shock vorticity disturbance which is amplified by the exothermic reaction, and acoustic disturbances whose amplitude decays for trailing subsonic flow and remains constant for trailing supersonic flow. Buckmaster[23] has also recently considered the stability of oblique detonations in the large activation energy limit. He reaches the conclusion, with minor qualifications explained in the paper, that oblique detonations are always structurally unstable. The different stability conclusions of our study and Refs. 21–23 remain to be resolved but are likely due to the different magnitudes of activation energies considered.

Second, an interesting result is suggested by Figs.

6a,b. Here it is seen that the chemical reaction gives rise to an unfavorable pressure gradient on the wedge surface in a region stretching from the wedge tip to the local pressure maximum. It is thus in principle possible that when boundary layer effects are modelled, this unfavorable pressure gradient could give rise to boundary layer separation from the wedge surface. Should this result extend to multicomponent mixtures, this boundary layer separation could give rise to an enhanced mixing rate.

Third, the asymptotic solution could be useful in boundary condition specification for numerical models. Though the reason for the pressure oscillations noted in Fig. 6b is not established, one explanation is that the imposed zero gradient boundary condition, which is not precisely correct, generates waves which propagate into the computational domain. As the asymptotic solution establishes that the gradients at these points are non-zero, the numerical solution could be improved by using the asymptotic solution to estimate conditions at the outflow boundary.

We lastly comment on the comparison of numerical and asymptotic results and the value of asymptotic results. Because of the conflicting criteria under which asymptotic and numerical models are valid representations of the full non-linear partial differential equations, one must exercise care to obtain meaningful comparisons. For example, the asymptotic results are strictly valid only in the limit as the incoming Mach number approaches infinity while the heat release is held fixed. There is a range in parameter space under which one can obtain apparently reasonable asymptotic results by holding the Mach number fixed and increasing heat release. For heat release above a critical value, however, the assumptions of the asymptotics are violated and the solution breaks down. In contrast, the numerical method is not limited to small heat release. The results of this paper indicate that for small heat release numerical artifacts can distort and overwhelm physical flow features while the accuracy tends to improve with increasing heat release. Consequently, there is a limited region in parameter space in which both methods predict qualitatively similar solutions.

The design of future aerospace vehicles will require the use of multidimensional models of nonequilibrium processes which take place on many length scales. The ability of asymptotic methods to generate engineering results in these cases is quite limited. The real value of the asymptotic solution discussed here lies in its ability to serve as an effective benchmark for the numerical codes which will be required for these complex problems. The results shown in this paper provide one example of the fundamental soundness and minor shortcomings expected from any numerical code designed to predict high-speed, non-equilibrium flow. In order to better assess the many current numerical algorithms, it is recommended that the asymptotic results be adopted as a new standard.

Acknowledgements

This work was supported by the Jesse H. Jones Faculty Research Program and the NASA-ASEE Summer Faculty Fellowship Program. The authors would also like to thank Beverly Duncan and Shaye Yungster of NASA Lewis Research Center for assistance with the RPLUS code.

References

[1]Vincenti, W. G., "Linearized Flow Over a Wedge in a Nonequilibrium Oncoming Stream," *Journal de Mecanique*, Vol. 1, Jun. 1962, pp. 193–212.

[2]Capiaux, R., and Washington, M., "Nonequilibrium Flow Past a Wedge," *AIAA Journal*, Vol. 1, Mar. 1963, pp. 650–660.

[3]Lee, R. S., "A Unified Analysis of Supersonic Nonequilibrium Flow over a Wedge: I. Vibrational Nonequilibrium," *AIAA Journal*, Vol. 2, Apr. 1964, pp. 637–646.

[4]Pratt, D. T., Humphrey, J. W., and Glenn, D. E., "Morphology of a Standing Oblique Detonation Wave," AIAA Paper 87-1785, Jun. 1987.

[5]Hertzberg, A., Bruckner, A. P., and Bogdanoff, D. W., "Ram Accelerator: A New Chemical Method for Accelerating Projectiles to Ultrahigh Velocities," *AIAA Journal*, Vol. 26, Feb. 1988, pp. 195–203.

[6]Witcofski R., Scallion W., and Carter, D., "An Advanced Hypervelocity Aerophysics Facility: A Ground-Based Flight-Test Range," AIAA Paper 91-0296, Jan. 1991.

[7]Bogdanoff, D. W., and Brackett, D. C., "A Computational Fluid Dynamics Code for the Investigation of Ramjet-in-Tube Concepts," AIAA Paper 87-1978, Jun. 1987.

[8]Fujiwara, T., Matsuo, A., and Nomoto, H., "A Two-Dimensional Detonation Supported by a Blunt Body or Wedge," AIAA Paper 88-0098, Jan. 1988.

[9]Wang, Y. Y., Fujiwara, T., Aoki, T., Arakawa, H., and Ishiguro, T., "Three-Dimensional Standing Oblique Detonation Wave in a Hypersonic Flow," AIAA Paper 88-0478, Jan. 1988.

[10]Cambier, J.-L., Adelman, H. G., and Menees, G. P., "Numerical Simulations of Oblique Detonations in Supersonic Combustion Chambers," *Journal of Propulsion and Power*, Vol. 5, Jul.-Aug. 1989, pp. 482–491.

[11]Cambier, J.-L., Adelman, H. G., and Menees, G.

P., "Numerical Simulations of an Oblique Detonation Wave Engine," *Journal of Propulsion and Power*, Vol. 6, May-Jun. 1990, pp. 315–323.

[12]Yungster, S., "Numerical Study of Shock-Wave/Boundary Layer Interactions in Premixed Hydrogen-Air Hypersonic Flows," AIAA Paper 91-0413, Jan. 1991.

[13]Yungster, S., Eberhardt, S., and Bruckner, A. P., "Numerical Simulation of Hypervelocity Projectiles in Detonable Gases," *AIAA Journal*, Vol. 29, Feb. 1991, pp. 235–241.

[14]Pandolfi, M., Arina, R., and Botta, N., "Nonequilibrium Hypersonic Flows Over Corners," *AIAA Journal*, Vol. 29, Feb. 1991, pp. 235–241.

[15]Anderson, J. D., *Hypersonic and High Temperature Gas Dynamics*, McGraw-Hill, New York, 1989.

[16]Powers, J. M., and Stewart, D. S., "Approximate Solutions for Oblique Detonations in the Hypersonic Limit," to appear in the *AIAA Journal*, Sept. 1991.

[17]Yu, S.-T., Tsai, Y. L., and Shuen, J.-S., "Three-Dimensional Calculation of Supersonic Reacting Flows Using an LU Scheme," AIAA Paper 89-0391, Jan. 1989.

[18]Tsai, Y. L., and Hsieh, K. C., "Comparative Study of Computational Efficiency of Two LU Schemes for Non-Equilibrium Reacting Flows," AIAA Paper 90-0396, Jan. 1990.

[19]Shuen, J.-S., and Yoon, S., "Numerical Study of Chemically Reacting Flows Using a Lower-Upper Symmetric Successive Overrelaxation Scheme," *AIAA Journal*, Vol. 27, Dec. 1989, pp. 1752–1760.

[20]Fickett, W., and Davis, W. C., *Detonation*, Univ. California Press, Berkeley, 1979.

[21]Jackson, T. L., Kapila, A. K., and Hussaini, M. Y., "Convection of a Pattern of Vorticity Through a Reacting Shock Wave," *Physics of Fluids A*, Vol. 2, July 1990, pp. 1260–1268.

[22]Lasseigne, D. G., Jackson, T. L., and Hussaini, M. Y., "Non-Linear Interaction of a Detonation/Vorticity Wave," NASA Contractor Report 187550, ICASE Report No. 91-34, April 1991.

[23]Buckmaster, J., "The Structural Stability of Oblique Detonation Waves," *Combustion Science and Technology*,Vol. 72, 1990, pp. 283–296.

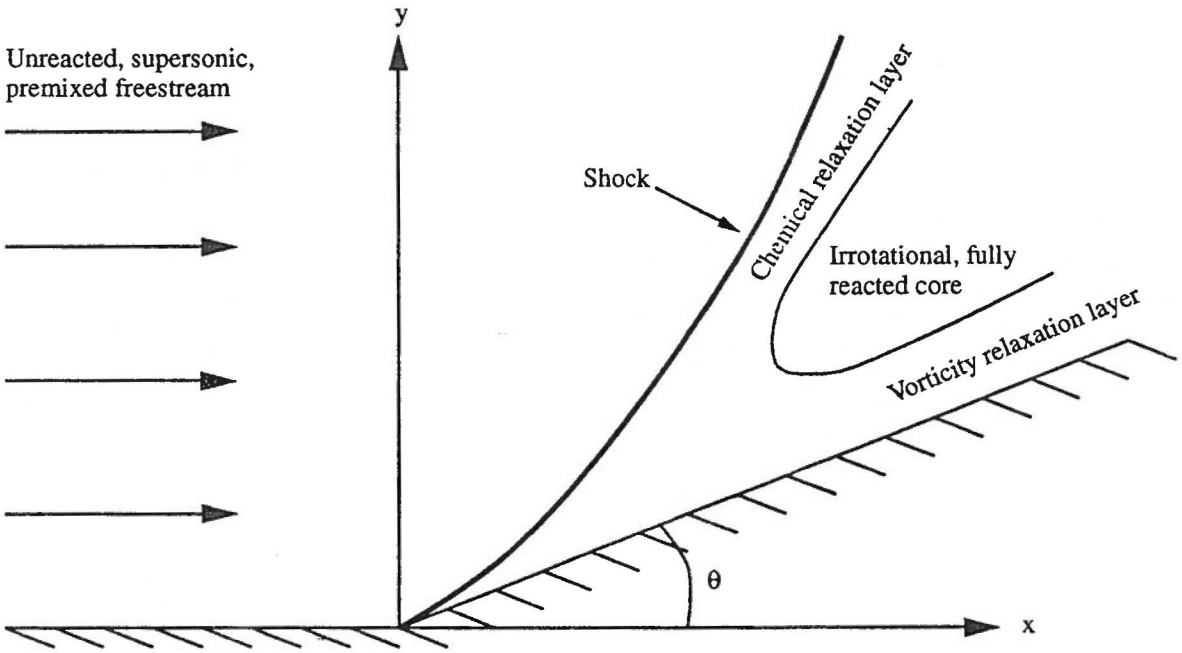

Fig. 1 Generic, inviscid, non-equilibrium, two-dimensional, supersonic flow over a wedge.

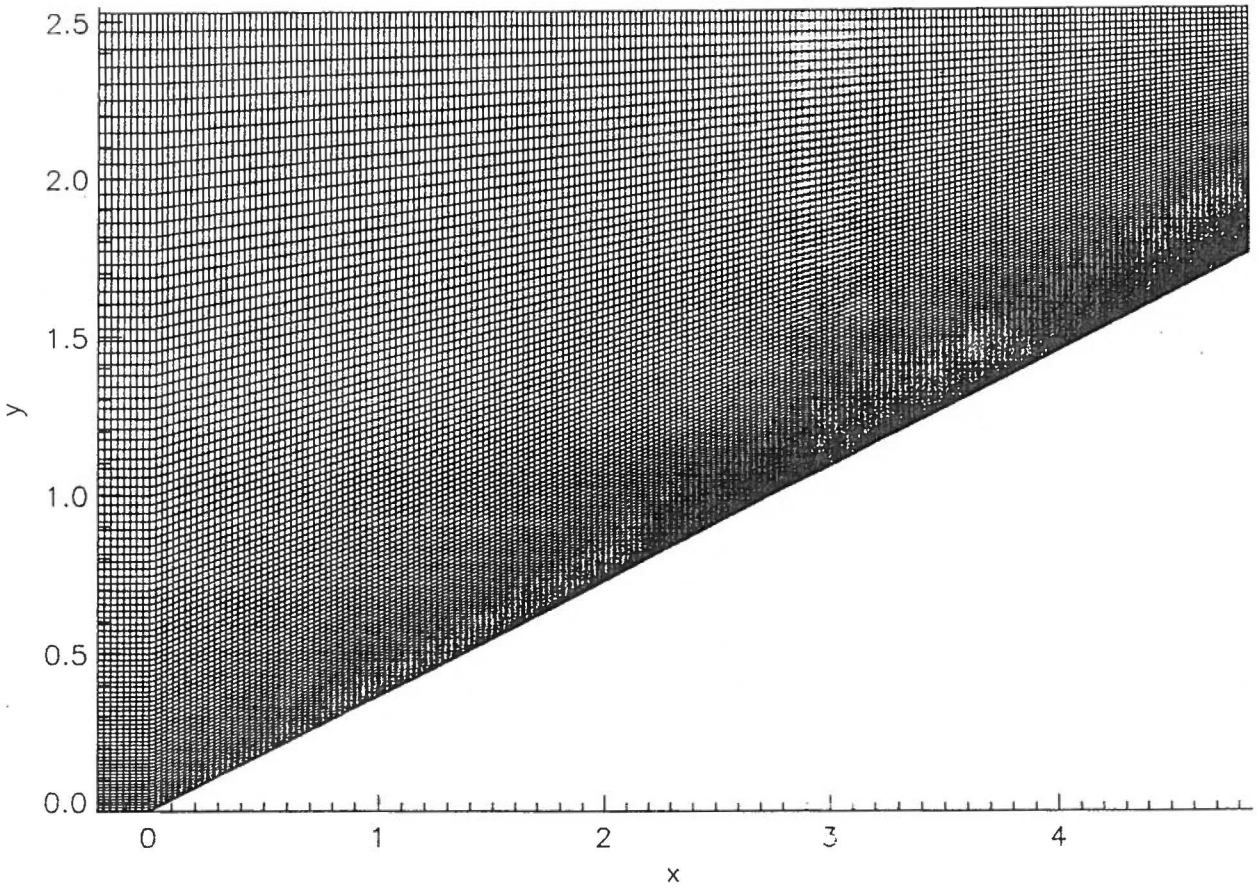

Fig. 2 Computational mesh of cell centers used in numerical calculations (199 by 99).

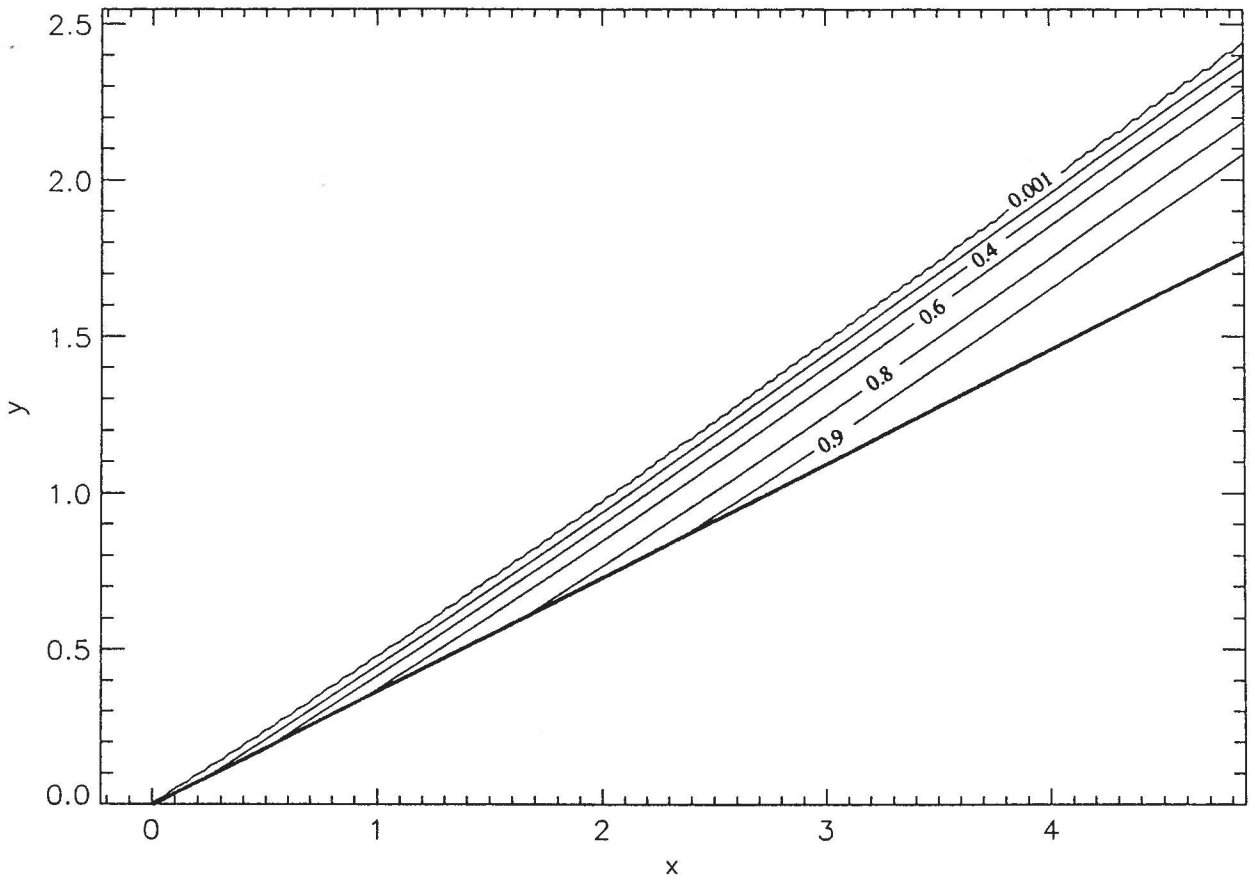

Fig. 3a Product mass fraction (λ) for asymptotic solution of case 1, q = 10.

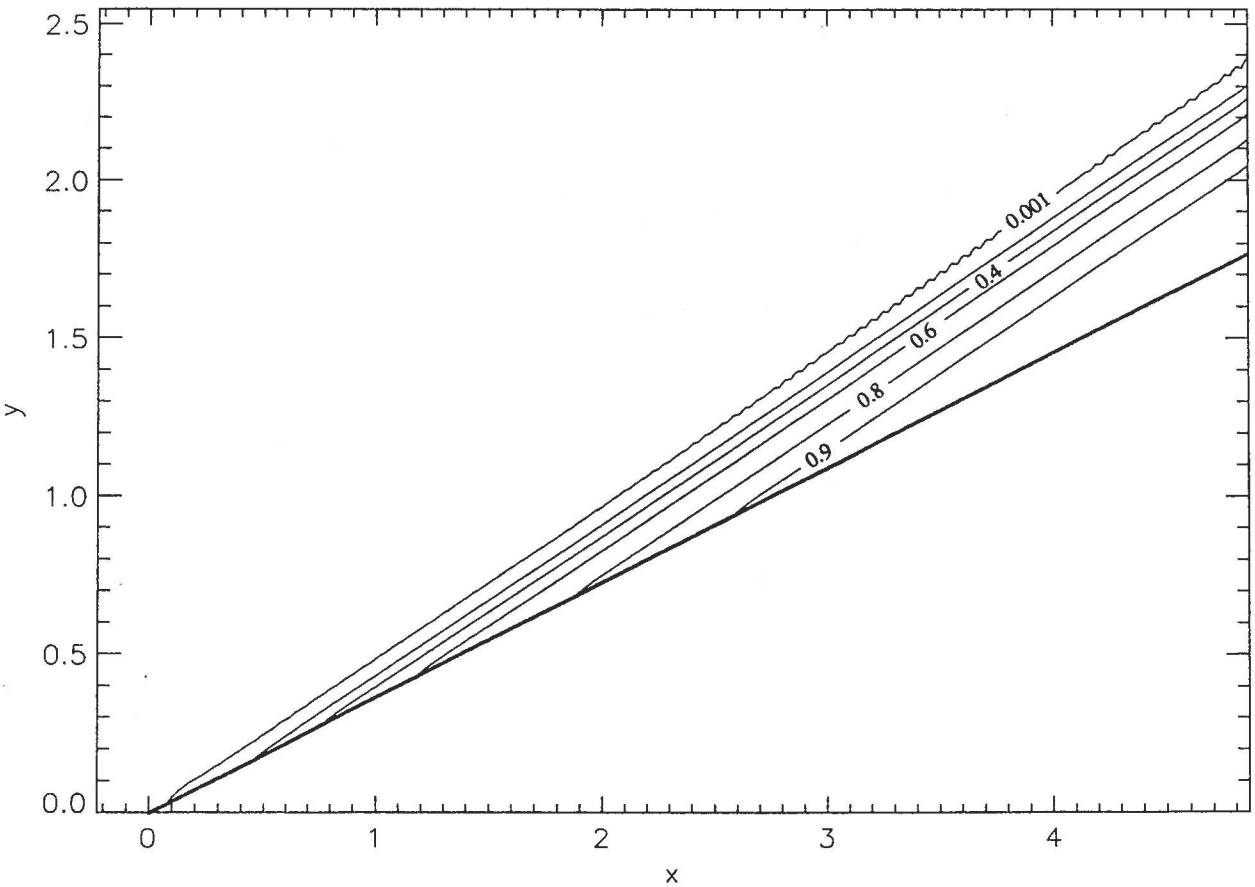

Fig. 3b Product mass fraction (λ) for numerical solution of case 1, q = 10.

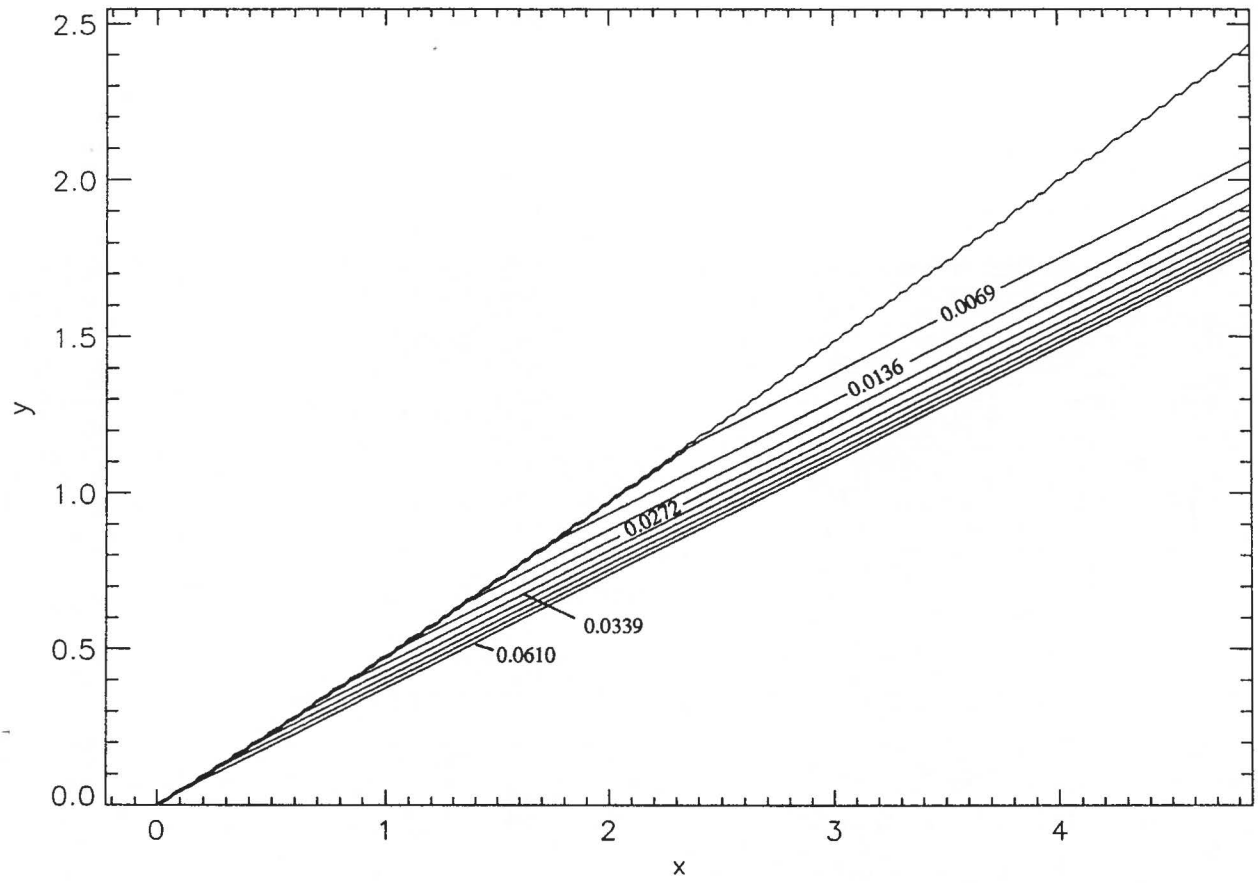

Fig. 4a Vorticity (ω_z) contours for asymptotic solution of case 1, q = 10.

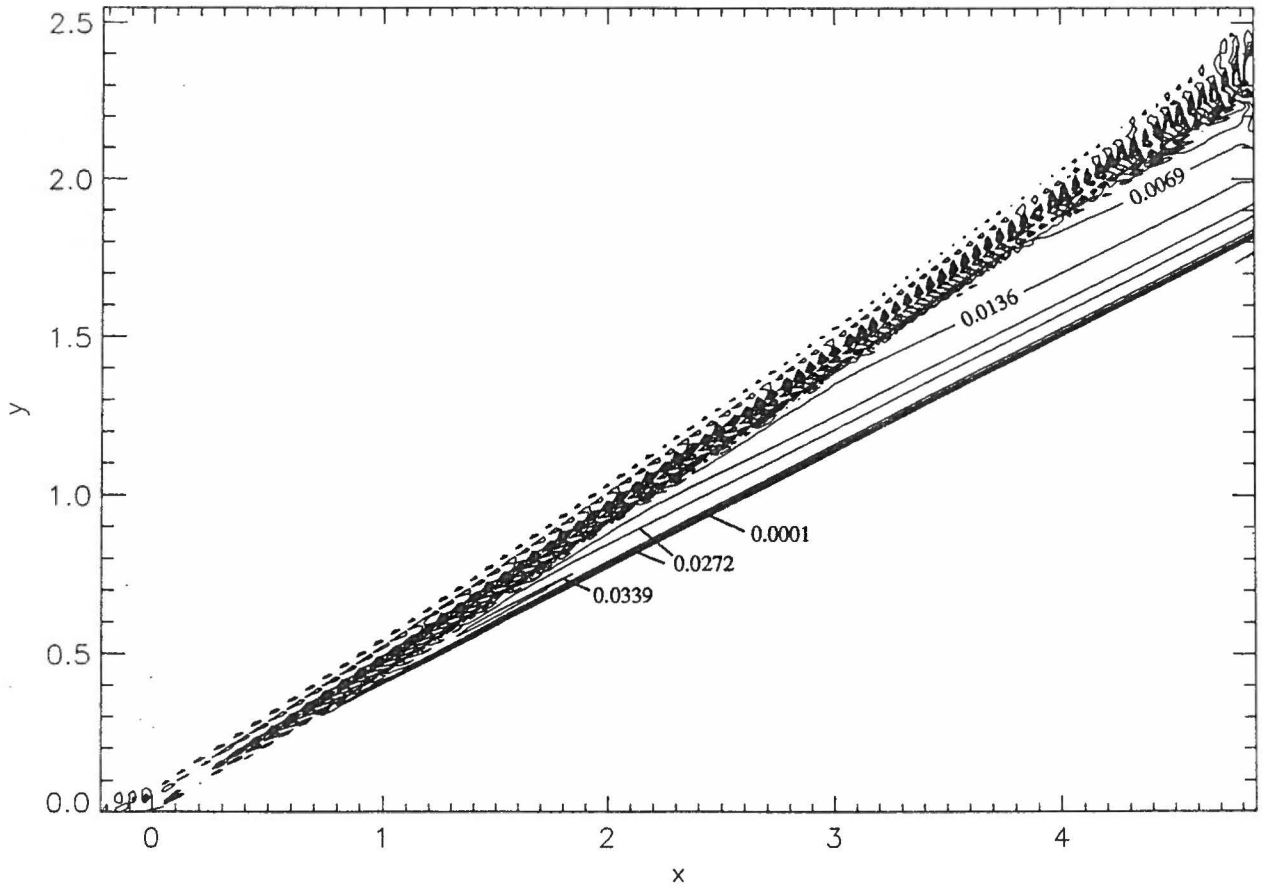

Fig. 4b Vorticity (ω_z) contours for numerical solution of case 1, q = 10.

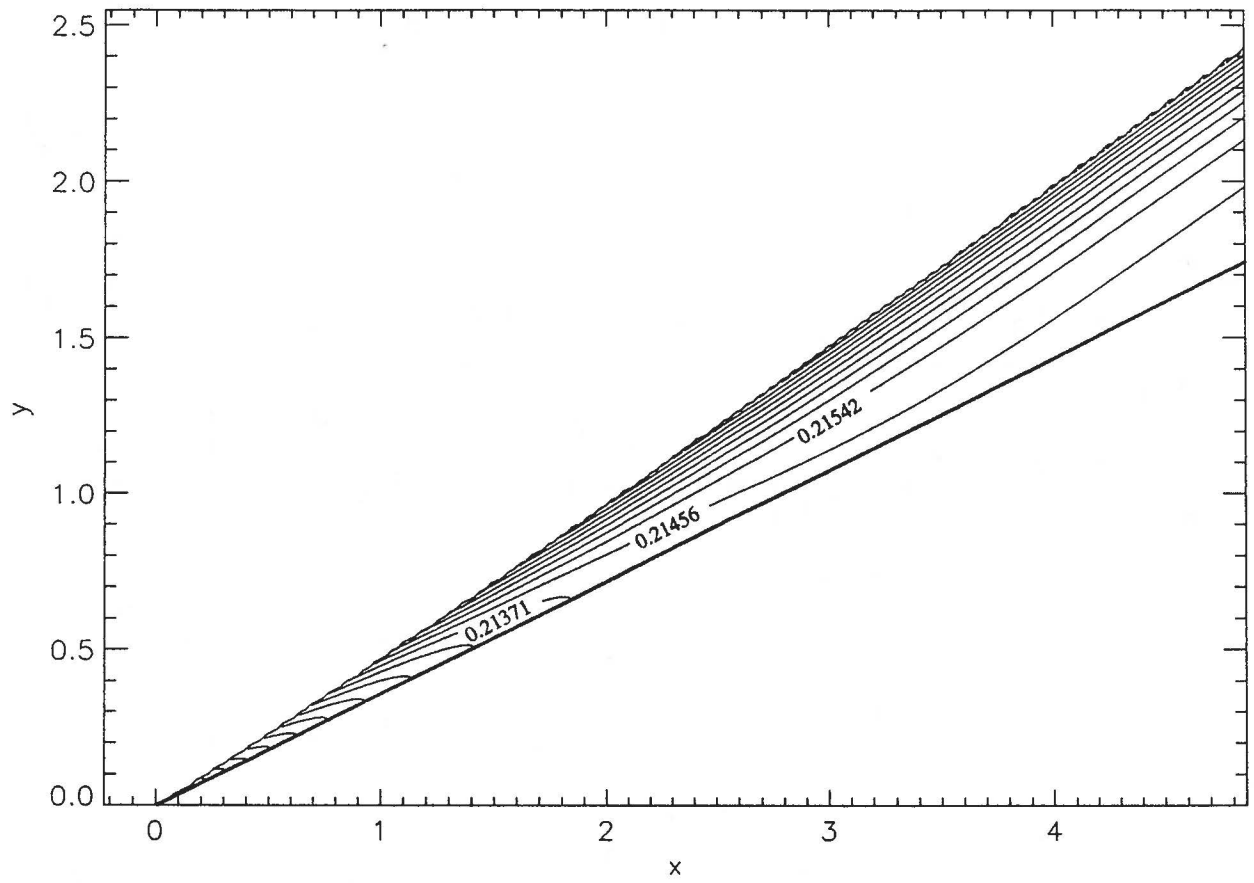

Fig. 5a Pressure (P) contours for asymptotic solution of case 1, q = 10.

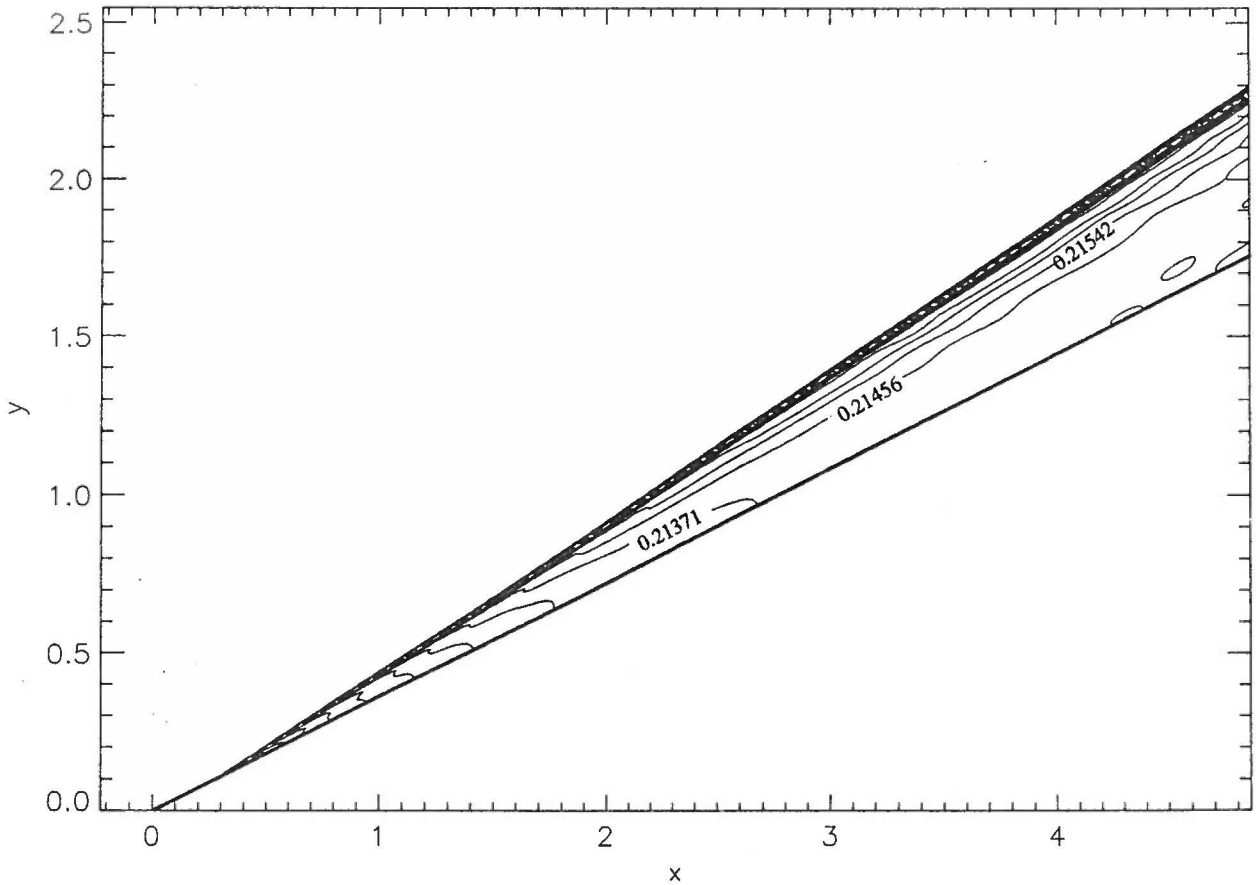

Fig. 5b Pressure (P) contours for numerical solution of case 1, q = 10.

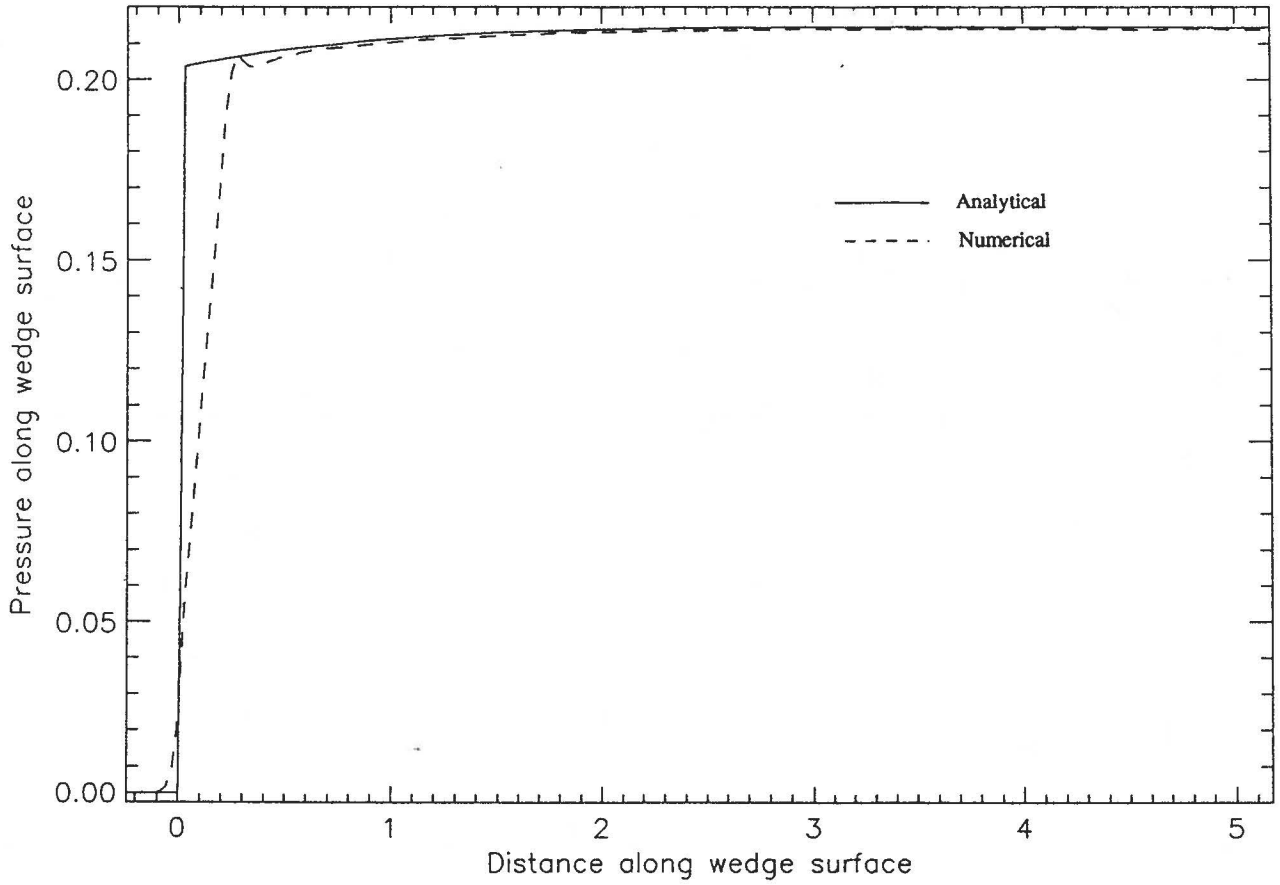

Fig. 6a Asymptotic and numerical wedge surface pressure predictions for case 1, q = 10.

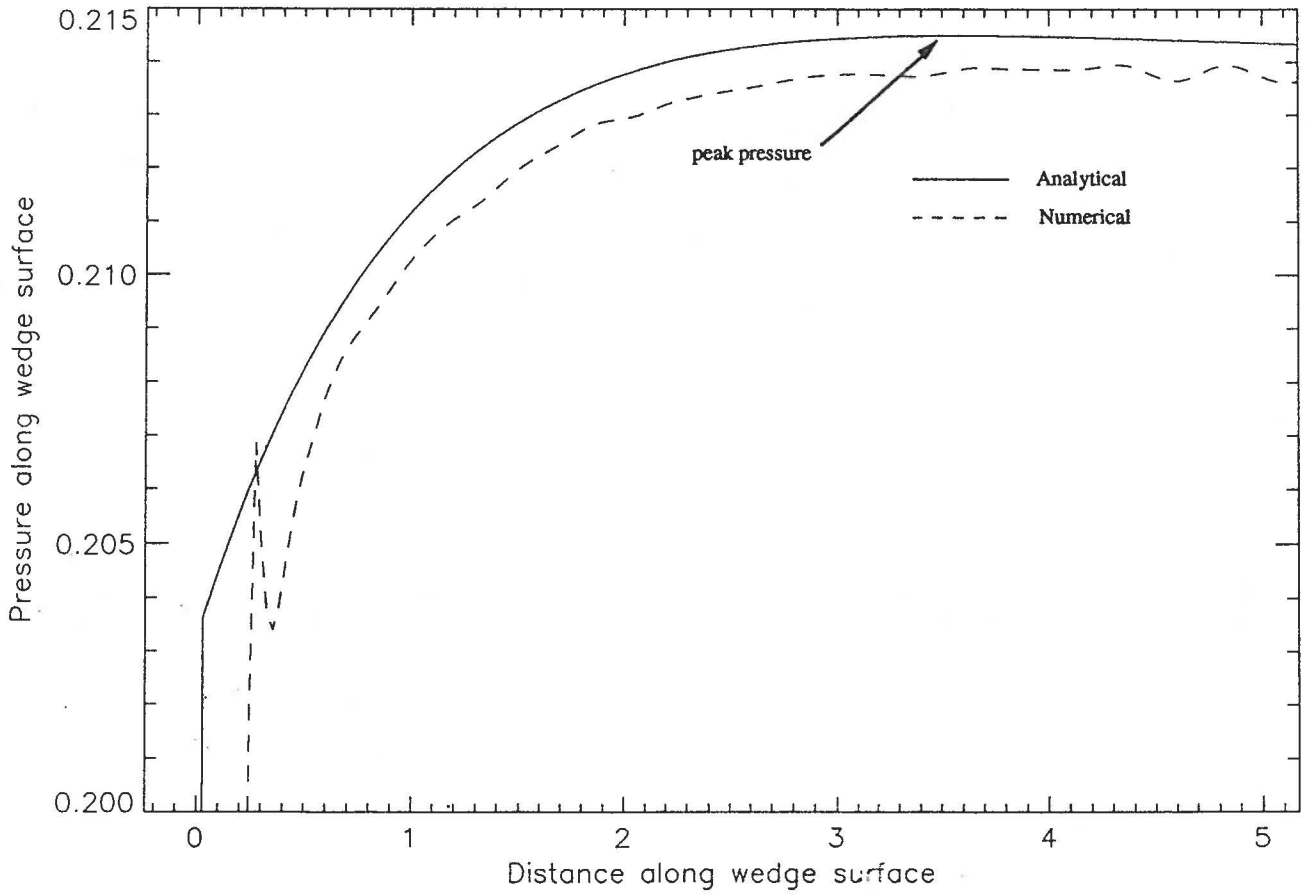

Fig. 6b Asymptotic and numerical wedge surface pressure predictions, expanded view, for case 1, q = 10.

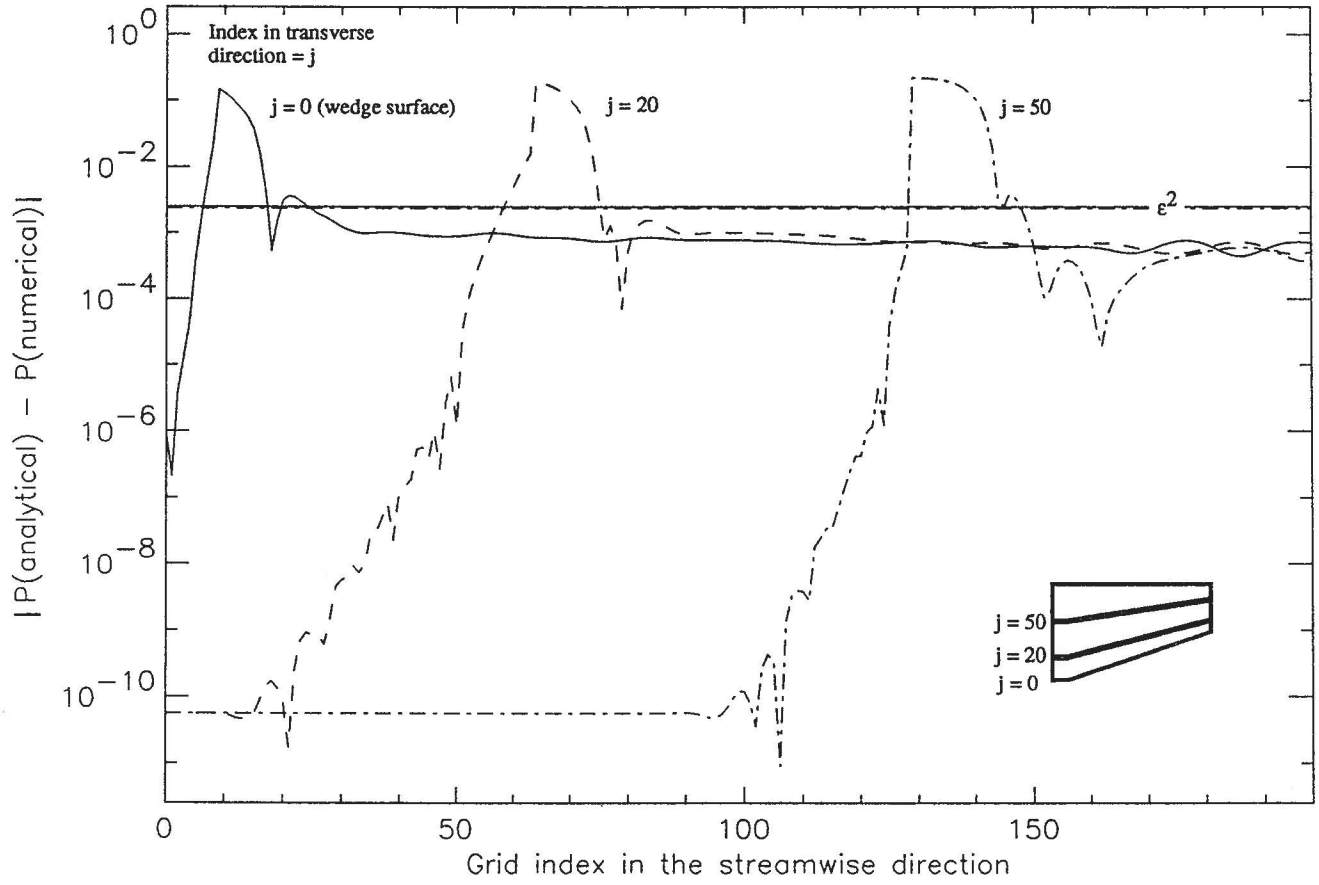

Fig. 6c Absolute value of the difference between asymptotic and numerical pressure compared with truncation error for case 1, q = 10.

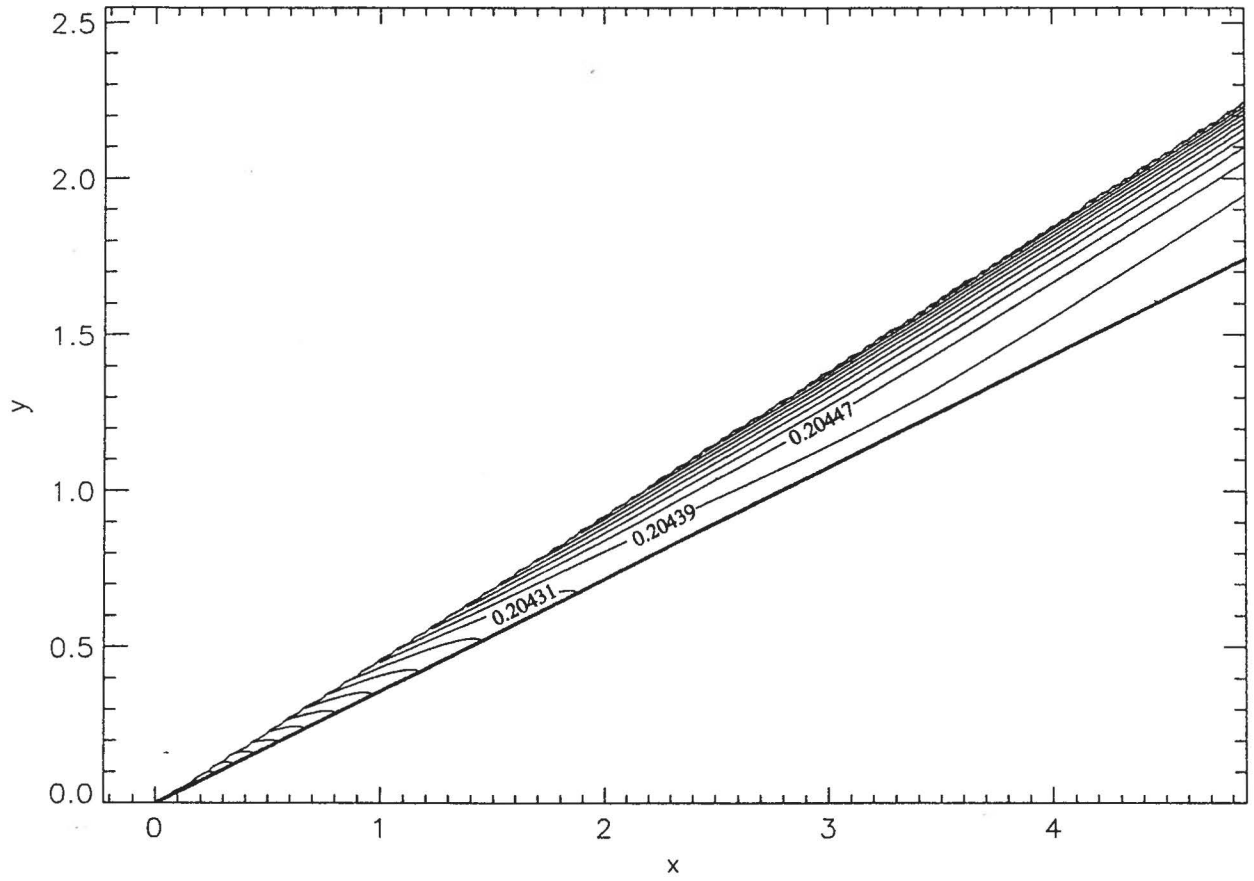

Fig. 7a Pressure (P) contours of asymptotic solution for case 2, q = 1.

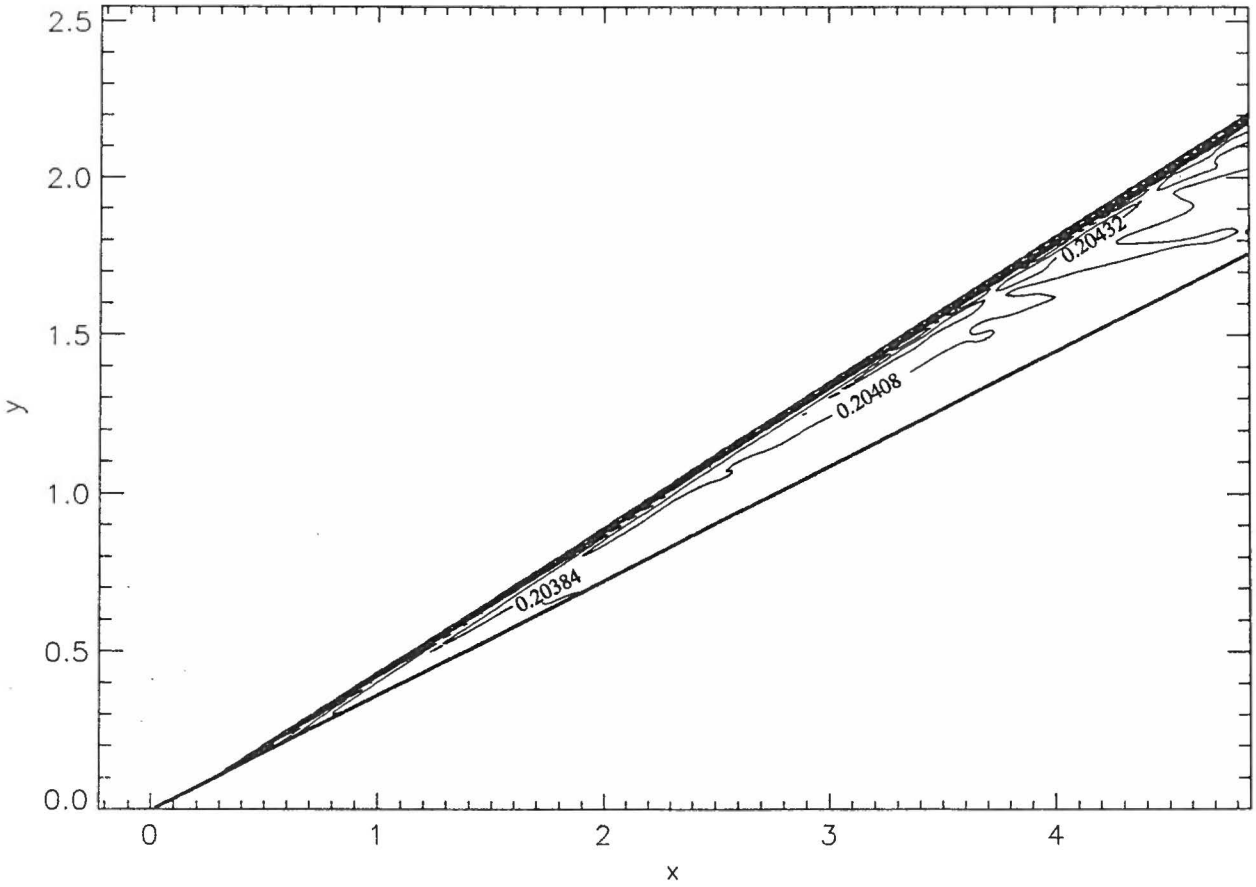

Fig. 7b Pressure (P) contours of numerical solution for case 2, q = 1.